A non-resonant mass sensor to eliminate the “missing mass” effect during mass measurement of biological materials

V. Shrikanth, and M. S. Bobji

Citation: Review of Scientific Instruments **85**, 105006 (2014); doi: 10.1063/1.4899201
View online: https://doi.org/10.1063/1.4899201
View Table of Contents: http://aip.scitation.org/toc/rsi/85/10
Published by the American Institute of Physics

A non-resonant mass sensor to eliminate the "missing mass" effect during mass measurement of biological materials

V. Shrikanth and M. S. Bobji[a)]
Department of Mechanical Engineering, Indian Institute of Science, Bangalore 560012, India

(Received 19 June 2014; accepted 12 October 2014; published online 28 October 2014)

Resonant sensors and crystal oscillators for mass detection need to be excited at very high natural frequencies (MHz). Use of such systems to measure mass of biological materials affects the accuracy of mass measurement due to their viscous and/or viscoelastic properties. The measurement limitation of such sensor system is the difficulty in accounting for the "missing mass" of the biological specimen in question. A sensor system has been developed in this work, to be operated in the stiffness controlled region at very low frequencies as compared to its fundamental natural frequency. The resulting reduction in the sensitivity due to non-resonant mode of operation of this sensor is compensated by the high resolution of the sensor. The mass of different aged drosophila melanogaster (fruit fly) is measured. The difference in its mass measurement during resonant mode of operation is also presented. That, viscosity effects do not affect the working of this non-resonant mass sensor is clearly established by direct comparison. © *2014 AIP Publishing LLC*. [http://dx.doi.org/10.1063/1.4899201]

I. INTRODUCTION

Mass measurement of viscoelastic/biological specimens is of growing importance starting from a unicellular organism to a multicellular insect and from femtoliter to a few milliliters of a liquid. Mass measurement of biological units is being done mainly using various balances such as triple/quadraple beam balance, Cahn electro-balance, and tuning fork mass sensors. These balances utilize different measurement techniques[1–3] like capacitive (resolution–10 mg), optical (0.01 mg), piezoresistive (10^{-3} mg), and piezoelectric (10^{-9} mg). Typically, the mass of an individual specimen is reported as an average of many specimens measured together.[4] This is done mainly due to the lack of resolution of the measuring instrument and also to avoid the effect of water vapour during the measurement. This results in the masking of individual variations. Population effects in statistical analyses are equivalent to block effects which are random in nature. A dynamically excited piezoelectric based mass measurement system is designed in this work to measure the tiny specimen individually.

Various piezoelectric based devices operated at resonance have been used for measuring mass of biological specimens such as quartz crystal micro-balance (QCM),[5] micro-resonators,[6] micro-cantilevers,[7] carbon nano-tubes.[8] These sensors can be broadly classified into two categories: (a) Resonating mechanical structures excited by external source, (b) Electronic oscillators with the oscillating element itself as the sensor.[9] Typically, cantilever beams[10–12] are used as mechanically resonating structures. A resolution of up to femtogram has been obtained by integrating microcantilever on a Silicon on Insulator substrate with doped top silicon layer. For integrated oscillating and sensing systems,[5,6] piezoelectric materials are invariably used. A new breed of microresonators make use of vibration localization in frequency mistuned microbeam resonators.[13] The sensitivity of the sensing element in such sensors depend on the location at which the mass is loaded.[14] Irrespective of the kind of the resonant sensor one uses to measure mass, the effect of viscosity/viscoelastic properties of the mass to be measured and the viscosity of the surrounding medium poses a difficulty in the measurement ("missing mass").[15] To overcome this difficulty, a new mass sensor has been developed in this work that operates in a non-resonant (off-resonance) mode.

Biological specimens are inherently viscoelastic in nature resulting in dissipation of energy in the specimen while measuring mass using resonant sensors. Mass is measured as a function of change in natural frequency of these sensors. This frequency shift happens due to two reasons: (a) change in the effective mass of the sensor (b) change due to viscosity and density of the surrounding fluid like air or water[16] as well as the viscous/viscoelastic material deposited on the electrode surface.[17,18] The change in the natural frequency due to viscous effects gives rise to a phenomenon called "missing mass" effect in liquid phase mass measurements where the actual mass cannot be accurately measured.[15] The inherent limitation of QCM for biological use is in distinguishing whether the response of QCM is either due to mass to be measured (adsorbed mass on the electrode surface) or due to viscosity/viscoelastic properties of the surrounding medium or both. Also, the behaviour and performance of resonant sensors/devices is dependent on the pressure of the surrounding medium.[19] The viscosity induced effect in the performance of a resonant sensor is existent mainly in two forms: squeeze film damping and drag force damping. Apart from viscous air damping, damping due to anchor losses, structural losses, thermo-elastic losses, and acoustic losses have to be taken into account to validate the performance of resonant sensors. The damping depends on the operating frequency as well and hence poses a great difficulty in calibration. In a QCM,[20] one of the frequently used resonant sensors for biological applications, inhomogeneous spread of the mass

[a)]Electronic mail: bobji@mecheng.iisc.ernet.in

placed/mounted on the electrode surface also contributes to the missing mass effect. Mass, when not spread homogeneously on the surface of the resonator, results in damped response due to localized vibration isolation.[21]

Resonant sensors have to be operated in vacuum, to minimize the effect of surrounding fluid on the performance of the sensor and hence cannot be used in mass measurement in biological applications as in mass detection of an insect or a fly. The sensor developed here overcomes the "missing mass" effect encountered while using resonators to measure mass of biological specimens by operating at a lower frequency compared to the first fundamental natural frequency of the system. The loss in measurement sensitivity due to this non-resonant operating frequency is compensated by using a highly sensitive Lock-in Amplifier. It is shown that this sensor can be used for mass measurements of viscoelastic/biological materials with a resolution of 0.1 μg and a wide range of 0.1 μg–1 g. The use of the sensor is demonstrated by measuring the mass of the egg, larvae, and the adult fly of drosophila melanogaster. The frequency response obtained from the experiments prove that the effects of viscoelastic properties of the specimen to be measured and viscosity of the surrounding medium does not contribute in any way to the measurement of its mass.

II. NON-RESONANT MASS SENSOR

The non-resonant sensor developed shown in Fig. 1 measures mass as a function of the inertial resistance required to oscillate it at a known driving frequency. To minimize the effect of damping, the oscillation frequency of the input signal is less than 2/5 th of the first fundamental natural frequency of the system. A piezoelectric element polarized in shear mode is used to detect the inertial resistance of the mass (m_a). This square sensing element of size $b = 5$ mm and thickness $h = 0.75$ mm is driven by another identical piezoelectric element.

The piezoelectric material used in the construction of the sensor is type PZT–5A with a dielectric constant (relative permittivity) $\varepsilon_r = 1725$. To minimize the charge leakage, lead resistance and to establish good electrical contact, the shear piezoelectric plates are sandwiched between copper-beryllium (Cu-Be) electrode plates of thickness 0.25 mm. The Cu-Be electrode plate has an area of 5 mm × 6 mm and shear piezo is aligned along the side that measures 5 mm. Use of Cu-Be instead of copper increases the stiffness of the sensor due to its higher value of Young's Modulus,[22] without compromising on the electrical conductivity. The interface of the piezo and the Cu-Be electrode plate is joined with a thin layer of conducting epoxy resin loaded with silver. The conducting epoxy resin is cured at 130 °C for a duration of 30 min. To ensure a good bonding between piezo and the Cu-Be electrode plate, they are held together by a tool maker's clamp. The actuator and sensing element are electrically isolated from each other by an alumina plate of thickness 0.15 mm and lateral area of 5 mm × 5 mm. Alumina is sandwiched between the Cu-Be electrode plates of the actuator element and sensing element by cyanoacrylate adhesive. Use of alumina (Al_2O_3) as an insulator provides high rigidity. The actuator element and

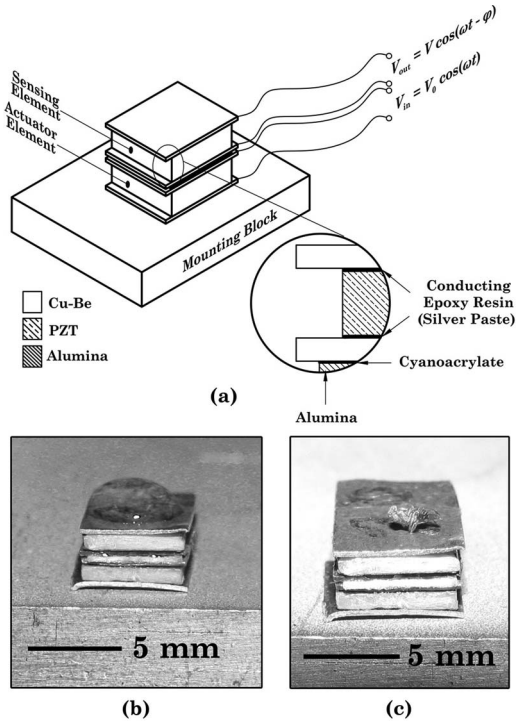

FIG. 1. (a) Mass sensor with actuator and sensing elements. The conducting epoxy resin layer thickness between Cu-Be electrode plate and piezo elements is about 50 μm. The piezo element has an edge of length $b = 5$ mm and a thickness of $t = 0.75$ mm. The Cu-Be electrode plate has a thickness of 0.25 mm, insulating alumina layer has a thickness of 0.15 mm. (b) 10 μl water drop mass being measured by the sensor. (c) A 60-day old drosophila fly mass being measured.

the sensing element piezo are now fixed to a mounting block with a layer of alumina between the electrode plate of the actuator element and the mounting block using cyanoacrylate.

The electrical connections to the piezoelectric elements are made by soldering silver wires (diameter of 150 μm) insulated with polyimide coating to the Cu-Be electrode plates. Standard BNC cable is used to connect the actuator element to the external voltage source, while low noise coaxial cable is used to connect the sensing element to the charge amplifier and signal conditioner. The capacitance of the sensing element is given by $\mathfrak{C} = \varepsilon_r \varepsilon_0 A/h$, where ε_r is the dielectric constant, ε_0 is the absolute permittivity, A is the lateral area, and h is the thickness of the piezo. The typical value of capacitance of the piezo used in the mass sensor shown in Fig. 1 is about 520 pF. As a consequence of this low capacitance, piezo material cannot store charges for a long time and hence discharge very quickly, with typical decay time of about 1.5 μs. Hence an actuator-sensor setup is developed to overcome the non-suitability of piezo material in static measurement.[23]

Care is taken to keep the conducting epoxy resin layer thickness to an optimal value[24] for better performance of the sensor. The effect of lead resistance can be eliminated by high quality of solders, while maintaining the temperature well below the curie temperature of 350 °C to prevent depolarization. The alignment of the polarization direction of the actuator and sensing element are parallel and in the same direction. Opposite and/or perpendicular alignment of the actuator and sensing element results in a cross talk of the displacements of the two piezos. As a consequence of this, the sensor output is

reduced by 40%. A thin layer of insulation made of acrylic is applied on the non-resonant mass sensor during the calibration and mass measurement to eliminate the charge leakage when any conducting material comes in contact with the Cu-Be electrode plate. The mass of the actuator-sensing element assembly excluding the mounting block is about 500 mg.

The driving oscillation amplitude input to the actuator element is varied by means of a high voltage amplifier (HVA) with adjustable gain. The non-resonant mass sensor is the transduction stage in the overall experimental setup and charge developed in this shear piezo sensing element is converted into voltage by an in-line charge amplifier (PCB 422E01). The in-line charge amplifier is driven by a signal conditioner (PCB 480B21) with adjustable gain of 1–100. The sensitivity of the in-line charge amplifier is 100 mV/pC. The voltage output from the sensor after charge to voltage conversion and amplification is measured by lock-in amplifier (LIA).

Stiffness and mass of the non-resonant mass sensor are the two main design constraints considered during the development and fabrication. Low stiffness brings down the natural frequency of the sensor and hence reduces the measurement range. Hence care should be taken to make the effective stiffness as high as possible and effective mass as low as possible without compromising the working of the non-resonant mass sensor. The conducting epoxy layer should not be thick so that the viscoelastic properties of the resin alters the performance of the mass sensor. At the same time it should not be too thin so that the strength of the epoxy layer is not sufficient to maintain electrical contact when operated at high frequencies. The electrode plate should cover the area of the piezo and not extend too much on either sides. As a result of bigger electrode plate, the effective mass of sensor increases, reducing the natural frequency of the sensor. A reduction in the natural frequency reduces the operating frequency range in non-resonant mode, hence reduces the range of measurement.

III. WORKING PRINCIPLE

The frequency response of a harmonically forced vibration system[25,26] clearly demarcates the stiffness controlled region and damping controlled region. The region where damping effects are negligible is called the stiffness controlled region. For a given value of stiffness and mass, the variation in the amplitude of the vibration system for varying values of the damping ratio ζ is noticeable for a ratio of $\omega/\omega_n \geq 0.4$. The variation in the amplitude is very small for $\omega/\omega_n \leq 0.4$ even when the damping ratio ζ is varied between 0 and 1. The effect of damping caused due to the viscosity of the surrounding air medium and viscoelastic properties of the mass to be measured is negligible when the sensor is operated under ambient conditions.

The actuator element shown in Fig. 1 undergoes an elastic deformation when a voltage is applied along the direction of polarization. The excitation voltage from HVA applied to the actuator element is of the form $V_{in} = V_0 \cos \omega t$, where V_0 is the rms voltage. The excitation frequency f ($\omega = 2\pi f$) is always above 1 kHz. When the voltage is applied to the shear piezo actuator element, it induces a displacement tangential to the surface along the polarization direction. The applied electric field and strain are related[23] by $\epsilon = d\vec{E}$, where ϵ is the strain, d is the piezoelectric charge constant, and $\vec{E}$ is the applied electric field. When shear piezo is used, ϵ is shear strain γ, d is d_{15}, piezoelectric charge constant for shear mode and $\vec{E} = V_{in}/h$, where h is the thickness of piezo. Neglecting the internal damping of the piezoelectric material and external damping of the system, the displacement ($a(t)$) of the actuator element in shear mode of operation due to a sinusoidal signal being applied is

$$a(t) = \mathrm{Re}\{a_0 e^{i\omega t}\}, \tag{1}$$

where $a_0 = d_{15} V_0$ is the excitation amplitude.

The sensing element fixed on the actuator element is moved by a distance that is equal to the elastic deformation of the actuator element. Due to this elastic deformation of the shear piezo actuator element and the inertia of the sensing element, a charge of $q_2 = \mathfrak{C}_2 V_2$ is generated in the sensing element, where $\mathfrak{C}_2$ is the capacitance of the sensing element. Using (1), the voltage output of the sensing element V_2 can be written as $\Delta y/d_{15}$, where Δy is the relative displacement of sensing element with respect to actuator element. The charge now becomes $q_2 = \mathfrak{C}_2 \Delta y/d_{15}$. The sensitivity of the in-line charge amplifier used in the transduction stage is 100 mV/pC. The voltage output of the sensing element measured by the lock-in amplifier is given by $V_{out} = q_2 \times 100$ mV.

The measurement of the mass (m_a) by the sensing element is accomplished due to the change in effective mass of the sensor. The voltage output from the sensing element in the sensor is of the form $V_{out} = V \sin(\omega t - \phi)$, ϕ being the phase difference between V_{in} and V_{out}. The undamped natural frequency of a single shear piezo is 647 kHz. The two damped natural frequencies of the sensor are $f_{d_1} = 20.1$ kHz and $f_{d_2} = 49.4$ kHz.

Mass measurement can be carried out between a frequency range of 1–5 kHz to safely work in the non-resonant mode of operation. For a fixed amplitude and frequency of the input voltage (V_{in}), the response and behavior as well as the sensitivity of the non-resonant mass sensor varies with varying the lateral area and thickness of the shear piezos used in the construction of the sensor. The dependence of the sensor output on the geometry of piezos is discussed in Sec. IV.

IV. LUMPED MODEL OF THE SENSOR

The piezo can be modeled as a lumped spring-mass-damper system. As shown in Fig. 2, the actuator element and sensing element are modeled as springs with mass.[26] The model describes the non-resonant mass sensor to be a statically coupled two degree of freedom (2-DOF) system. An equivalent force F due to the input voltage V_{in} is considered. The excitation voltage applied across the actuator element is proportional to a force F of amplitude $F_0 = AGd_{15}V_0/h$, given by

$$F = \mathrm{Re}\{F_0 e^{i\omega t}\}, \tag{2}$$

where G is the Rigidity Modulus of the piezo material, A is the lateral area, and h is the thickness of the piezo. The stiffness

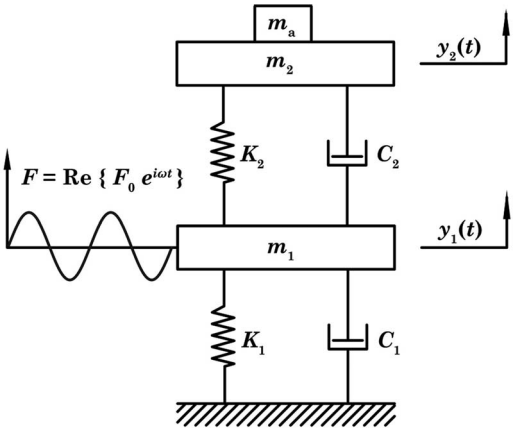

FIG. 2. Representative lumped model of the mass sensor. The forcing term F is the equivalent force acting on the system due to the applied voltage to the actuator element, m_a is the mass to be measured by the sensing element.

of the actuator element and sensing element is given by $K_1 = GA_1/h_1$ and $K_2 = GA_2/h_2$, respectively.

The terms K_1, C_1, m_1 and K_2, C_2, m_2 in Fig. 2 are the effective stiffness, effective damping coefficient, and effective mass of the actuator element and sensing element, respectively. $y_1(t)$ and $y_2(t)$ are the displacements of the actuator element and sensing element, respectively. The mass m_1 is the combined mass due to actuator element, insulating alumina layer, sensing element, Cu-Be electrode plates, super glue, and conducting epoxy resin. Similarly, m_2 is due to sensing element, epoxy, and Cu-Be electrode plate at the top of the sensor piezo.

With the mass to be measured m_a, m_1, and m_2 can be written as $m_1 + m_a = m_1'$ and $m_2 + m_a = m_2'$. The differential equations of motion of the non-resonant mass sensor are

$$\ddot{y}_1 = \frac{F}{m_1'} - 2\zeta\omega_{11}\dot{y}_1 - \omega_{11}^2 y_1 + 2\zeta\omega_{21}(\dot{y}_2 - \dot{y}_1) + \omega_{21}^2(y_2 - y_1),$$
$$\ddot{y}_2 = -2\zeta\omega_{22}(\dot{y}_2 - \dot{y}_1) - \omega_{22}^2(y_2 - y_1), \tag{3}$$

where $\omega_{11}^2 = K_1/m_1'$, $\omega_{21}^2 = K_2/m_1'$, and $\omega_{22}^2 = K_2/m_2'$. Assuming the displacements y_1 and y_2 to be harmonic such that $y_1 = Y_1 e^{i(\omega t+\phi_1)}$ and $y_2 = Y_2 e^{i(\omega t+\phi_2)}$, $\dot{y}_1 = i\omega y_1$, $\dot{y}_2 = i\omega y_2$, $\ddot{y}_1 = -\omega^2 y_1$, and $\ddot{y}_2 = -\omega^2 y_2$. The combined mass, stiffness and damping matrix is denoted by $\mathbf{D}$, the displacement vector $\mathbf{Y}^{\mathrm{T}} = \{y_1 \quad y_2\}$ and force vector $\mathbf{F}^{\mathrm{T}} = \{F/m_1' \quad 0\}$. Inverting the matrix $\mathbf{D}$ and pre-multiplying it on both sides of (3) in matrix form $\mathbf{DY} = \mathbf{F}$, the displacements obtained are

$$y_1 = \frac{A_{22}F}{m_1'\left(A_{11}A_{22} - A_{12}A_{21}\right)}, \tag{4}$$

$$y_2 = \frac{A_{21}F}{m_1'\left(A_{11}A_{22} - A_{12}A_{21}\right)}, \tag{5}$$

where $A_{11} = -\omega^2 + i2\zeta\omega(\omega_{11} + \omega_{21}) + \omega_{11}^2 + \omega_{21}^2$, $A_{12} = -(i2\zeta\omega\omega_{21} + \omega_{21}^2)$, $A_{21} = -(i2\zeta\omega\omega_{22} + \omega_{22}^2)$, and $A_{22} = -\omega^2 + i2\zeta\omega\omega_{22} + \omega_{22}^2$. (4) and (5) are steady state solutions for displacement of actuator element and sensing element, respectively, in general for any geometry. The system in Fig. 2 when not under any influence of damping and forcing, the free oscillations give information of the two natural frequencies[25,26] ω_{n_1} and ω_{n_2}. When $m_a = 0$ and zero external forcing, the solution of the characteristic equation for the case of no damping, gives the two natural frequencies ω_{n_1} and ω_{n_2},

$$\omega_{n_{1,2}}^2 = \frac{1}{2}\Big[\omega_{11}^2 + \omega_{21}^2 + \omega_{22}^2 \pm \sqrt{\left(\omega_{11}^2 + \omega_{21}^2 + \omega_{22}^2\right)^2 - 4\omega_{11}^2\omega_{22}^2}\Big]. \tag{6}$$

Since the actuator element and sensing element are identical, the stiffness of the two piezos is $K_1 = K_2 = K = 8 \times 10^8$ N/m. The effective masses of actuator element and sensing element are $m_1 = 550 \times 10^{-6}$ kg and $m_2 = 200 \times 10^{-6}$ kg. Substituting K_1, K_2, m_1, and m_2 in (6), the two natural frequencies are $f_{n_1} = 157.62$ kHz and $f_{n_2} = 387.5$ kHz where $f_{n_{1,2}} = \omega_{n_{1,2}}/2\pi$. Using the relation $\omega_d = \sqrt{1-\zeta^2}\,\omega_n$ and comparing the resonant frequencies obtained from the experimental frequency response, the damping ratio ζ is found to be 0.992. The time dependent part of the solution[27] in (4) and (5) gives the phase relationship between the applied force (voltage) and displacement of the actuator element, as well as that between the applied force (voltage) and displacement of the sensing element.

The relative displacement of the sensing element with respect to the actuator element is $\Delta y = y_2 - y_1$ and the generated charge due to shear strain is $q_2 = C_a\Delta y/d_{15}$. Neglecting the damping terms and substituting for lateral area A, thickness of the piezo h and m_2' in (4) and (5), the charge generated per unit input voltage can be approximated to

$$\frac{q_2}{V_{in}} = \frac{(m_2 + m_a)\omega^2 GA^2\varepsilon_0\varepsilon_r}{m_1'm_2'h^2\omega^4 - 2m_2'GAh\omega^2 + G^2A^2}. \tag{7}$$

The total voltage output of the sensor from the charge amplifier with a sensitivity of 100 mV/pC is

$$V_{out} = 100\, q_2\, V_{in}. \tag{8}$$

With $m_1'm_2'h^2\omega^4 - 2m_2'GAh\omega^2 \ll G^2A^2$ and substituting for m_1' and m_2', (8) can be rewritten as $V_{out} = S_t m_a + R$, where $S_t = 0.045\, V_{in}$ is the theoretical sensitivity of the sensor and $R = 102.8\, V_{in}$ is the voltage output of the sensor when $m_a = 0$. Substituting the values of m_1, m_2, G, A, h, ω, ε_0, and ε_r in (8),

$$V_{out} = \left(0.045m_a + 102.8\right) \times V_{in}. \tag{9}$$

The lumped model given above predicts the performance of the non-resonant mass sensor to a good degree of agreement with the experimental results. Section V presents the experimental evidence of the working of the sensor. Also, the sensor performance for varying geometry, experimental frequency response, and its application in the measurement of mass of drosophila melanogaster, its egg and larvae.

V. RESULTS AND DISCUSSION

Fig. 3 shows the amplitude of the output signal against mass to be measured (m_a) using standard solid and liquid

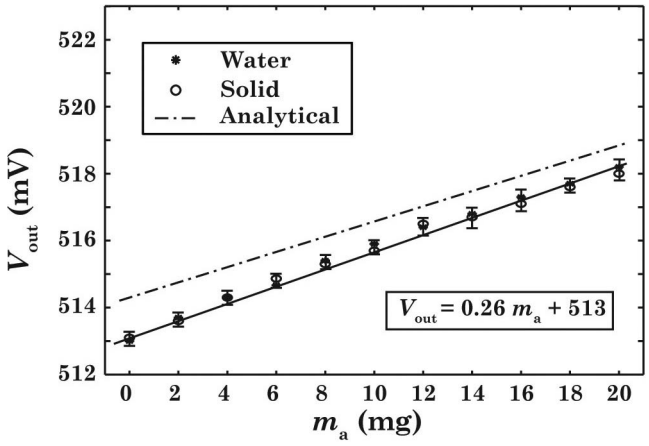

FIG. 3. Depiction of the linear variation in the output voltage of the non-resonant mass sensor corresponding to added mass m_a (0−20 mg) measured at input voltage $V_{in} = 5$ V, ambient temperature is 25 °C, excitation frequency $f = 1000$ Hz.

mass (water of density 1000 kg/m^3) during the calibration of the sensor. A vibrating tuning fork based weighing balance was used to establish the standard solid mass (aluminum discs). For liquid mass, mass of a known volume of water was measured. The mass measurements are carried out under the following conditions: input voltage $V_{in} = 5$ V, ambient temperature is 25 °C, excitation frequency $f = 1000$ Hz. The variation in the voltage output of the sensor corresponding to the mass to be measured m_a is monotonic for mass measurements done up to an operating frequency of 8 kHz. For any measurements made above an operating frequency of 10 kHz, the output voltage V_{out} with respect to m_a varied non-monotonically. Note that the first damped natural frequency is $f_{d_1} = 20.1$ kHz and for an operating frequency of $f = 8$ kHz, the ratio $\omega/\omega_n < 0.4$. The sensitivity of the sensor can be improved by increasing the voltage input (V_{in}) to the sensor.

The voltage output of the sensor for standard solid mass is given in Fig. 3. The monotonic variation in the voltage output corresponding to the mass to be measured is consistent for all operating frequencies up to 8 kHz. The deviation in the voltage output of the sensor due to the location of the placement of mass to be measured m_a is within the experimental limits. The solid mass is placed on the sensor by means of tweezers with insulation at the tip. The monotonic variation trend of the sensor output in Fig. 3 is $V_{out} = 0.26\, m_a + 513$.

Mass measurement of water (viscous/viscoelastic material) is carried out using the sensor developed. Now, it stands to reason whether the mass of a solid and an equal mass of a liquid when measured with this sensor measures the same. It is found out that the amplitude of the voltage output of the sensor for water is the same as that of the solid mass. The state/phase of the measured mass does not in anyway contribute to the outcome of the non-resonant mass sensor.

The voltage output of the sensor corresponding to the mass to be measured m_a is compared with the predicted results from the lumped model and a reasonably good agreement between the two is found. Theoretically, there is no variation in the response of the sensor when the damping ratio ζ is varied between 0 and 1 in the non-resonant mode. Writing equivalent

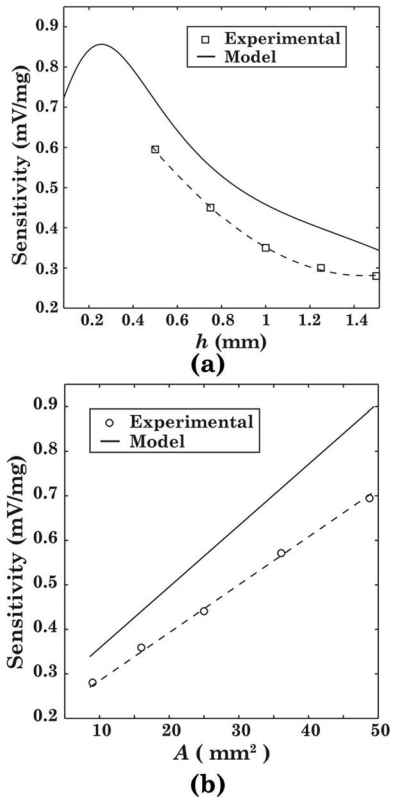

FIG. 4. (a) Variation in the sensitivity of the non-resonant mass sensor when the thickness of the piezos are varied for a fixed amplitude and frequency of operation. (b) Linear trend observed in sensitivity of mass sensor due to a change in the lateral area of the actuator and sensing elements.

densities ρ_1 and ρ_2 for actuator and sensing elements, respectively, so that $m_1' = \rho_1 Ah$ and $m_2' = \rho_2 Ah$, (8) can be written as

$$V_{out} = \frac{Ah}{\alpha h^4 - \beta h^2 + \gamma}, \tag{10}$$

where $\alpha = \rho_1 \omega^2 / 100 G \varepsilon_0 \varepsilon_r V_{in}$, $\beta = 2/100 \varepsilon_0 \varepsilon_r V_{in}$, and $\gamma = G/100 \rho_2 \omega^2 \varepsilon_0 \varepsilon_r V_{in}$.

The ratio of the charge generated per unit input voltage q_2/V_{in} is constant for a given geometry of the mass sensor. The charge generated by the sensing element q_2 as seen in (7) is directly proportional to the input voltage V_{in}. The sensitivity of the charge amplifier used in the transduction stage is 100 mV/pC. Theoretically, the sensitivity of the sensor is $0.045 \times (V_{in})$ mV/mg and the experimental sensitivity of the non-resonant mass sensor is $S = 0.057 \times (V_{in})$ mV/mg. Depending on the order of magnitude of the mass to be measured m_a, sensitivity can be varied by varying the input voltage (V_{in}) ranging from 1–300 V. This dynamically excited non-resonant miniature mass sensor is used to measure mass ranging from 0.1 μg–1 g. When the area and thickness of the piezo are altered, there is a corresponding change in the response of the sensor.

Fig. 4 shows the sensitivity of the sensor when the geometries of the actuator element and sensing element are varied. Results in Fig. 4(a) are for sensors with constant lateral area $A = 25$ mm^2. The thickness is varied in steps of 0.25 mm ($h = 0.5$, 0.75, 1, 1.25, and 1.5 mm). The thickness

of the actuator element and the sensing element are kept the same to have equal stiffness. An increase in the thickness of the piezo element increases the effective mass while reducing the stiffness of the sensor. Capacitance of the piezo element is increased when thickness is decreased. The analytical results plotted in Fig. 4 are independent of the damping ratio ζ. The thickness of both the piezos is varied equally. The sensitivity of the sensor increases with decreasing thickness of the piezo element. Analytical results predicted by (10) show a similar trend as observed in the experiments. The deviation of the results predicted by the model from that of the experimental results is due to the assumption that the damping ratio ζ is 0.

The results shown in Fig. 4(b) are for sensors having sides $b = 3$, 4, 5, 6, and 7 mm with a constant thickness of $h = 0.75$ mm. The experimental results indicate that as the lateral area of the piezo element is increased, there is a corresponding increase in the sensitivity of the sensor. Also, from (10) it is evident that the sensitivity of the sensor increases with increasing area. The effective mass and stiffness of the sensor as well as the capacitance of the piezo element all increase with increasing area. In all designs of the sensor, there is a monotonic increase in the variation of the voltage output of the sensor corresponding to m_a.

The variation in the sensitivity of the sensor corresponding to a change in the geometry of the piezo element used can be attributed to: (a) Change in the effective stiffness and effective mass of the sensor as the geometry of the piezo element is varied thus changing the sensitivity of the non-resonant mass sensor (b) Capacitance of the piezo changes with changing geometry and hence an increase or decrease in the amount of charge generated per unit input voltage. (10) gives the sensitivity of the sensor to be maximum when the thickness is 0.3 mm. Reducing the thickness further decreases sensitivity the sensitivity of the sensor. An optimum thickness that gives good sensitivity and ease of fabrication/construction can be arrived at from (10). The lateral area of the piezo element used in the sensor can be increased to a large value (≈100 mm) to increase the sensitivity. Based on the need of the sensor for a specific measurement the dimensions of the piezo elements can be suitably chosen from Fig. 4. An increase in the lateral area does not change the natural frequency when the piezo elements are operated in shear mode. Reduction in thickness increases the natural frequency. In both these cases, change in geometric dimensions increase the capacitance and hence increases the sensitivity of the sensor. The final design of the sensor used in the mass measurement of drosophila melanogaster has the following dimensions: $b = 5$ mm and $h = 0.75$ mm. The final design is arrived at keeping in mind the fabrication process. The same design is used to obtain the frequency response of the sensor and hence to determine the frequency range of operation in non-resonant mode.

Stiffness controlled region is necessary to determine the non-resonant mode of operation of the sensor. The frequency response of the sensor is obtained to ascertain the range of operation of the sensor and distinguish the stiffness controlled region. The frequency response also gives the operating frequency above which the viscosity/viscoelastic properties of the mass to be measured affect the measurements.

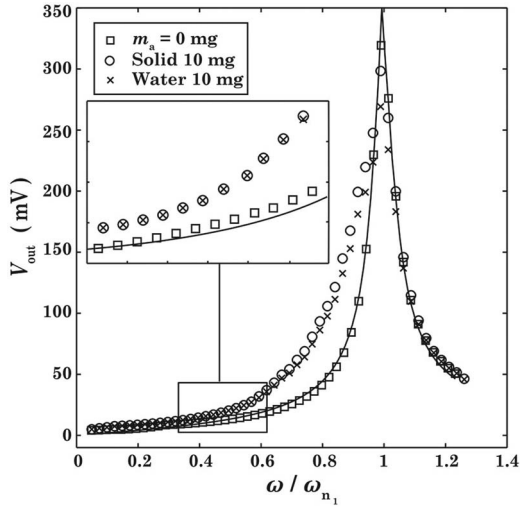

FIG. 5. Frequency response curve of the non-resonant mass sensor with and without the mass to be measured (m_a). The response when $m_a = 0$ is fit with nonlinear least squares derived from the analytical equations (4) and (5).

The experimental frequency response of the mass sensor is shown in Fig. 5. At first, the frequency response of the sensor is obtained when $m_a = 0$. The input voltage (V_{in}) is 1 V and the frequency is swept linearly from 1–100 kHz. A solid mass of 10 mg and water measuring 10 mg is placed on the sensor to get the frequency response. An appreciable change in the output voltage of the non-resonant mass sensor is evident in Fig. 5 between solid and liquid mass at $\omega/\omega_{n_1} = 1$. A shift in the natural frequency in case of water is noticeable which indicates a tiny amount of water to have evaporated over the period of the experiment. Irrespective of where the mass to be measured is placed on the sensor, the voltage output of the sensor is the same. In other words, output is not dependent on the location of the placement of mass unlike micro-cantilevers/resonators[28] as long as the dimension of the measured mass is less than or comparable with the size of the sensor.

The analytical frequency response is obtained without neglecting the damping terms in (4) and (5). The difference in the experimental and analytical results of the frequency response of the sensor is quite large in and around the region where $\omega/\omega_{n_1} = 1$. This is due to the assumption that the damping is linear in the system and no nonlinearity effects exist. The frequency response of the system of equations involving (4) and (5) gives the damped natural frequencies $f_{d_1} = 20.2$ kHz and $f_{d_2} = 49.6$ kHz for a value of $\zeta = 0.992$. These damped natural frequencies are in good agreement with the experimentally obtained ones of 20.1 kHz and 49.4 kHz.

The outcome of this frequency response reveals two things: (a) The difference in the voltage output of the sensor is very small for solid mass and water till the ratio of $\omega/\omega_{n_1} = 0.4$. The response of the sensor depends mainly on the stiffness of the system in the case of $\omega/\omega_{n_1} = 0.4$. Damping of the system due to viscosity/viscoelastic properties of the surrounding medium does not vary the output when solid and liquid masses are measured, hence irrespective of the

state/phase of the mass being measured the output remains the same. (b) As the operating frequency is increased to a ratio of $\omega/\omega_{n_1} > 0.4$, the output of the sensor gradually starts to differ for solid and liquid masses. A significant difference in the voltage output of the sensor is evident in and around the resonance region (damping controlled region). The analytical frequency response is different from the experimental response for values of $\omega/\omega_{n_1} > 0.4$. So, the model presented in Sec. IV can be used to predict the response of the sensor in the non-resonant mode (stiffness controlled region), when the operating frequency is very much less than the first fundamental natural frequency. For a 2-DOF system, the frequency response up to the first natural frequency can be given by the equation

$$|V_{out}|^2 = \frac{\mathcal{A}\omega^2}{(\mathcal{B}-\omega^2)^2 + \mathcal{B}\mathcal{C}\omega^2}, \tag{11}$$

(11) is the nonlinear least squares function in which $\mathcal{A}$, $\mathcal{B}$, and $\mathcal{C}$ are the fitting constants and f is the operating frequency. The constants $\mathcal{A} = (AGV_{in}d_{15}/hm_2\varepsilon_0\varepsilon_r)^2$, $\mathcal{B} = \omega_{d_1}^2$, and $\mathcal{C} = 4\zeta^2$ are used to find out the piezoelectric charge constant d_{15}, first damped natural frequency f_{d_1} and damping ratio ζ, respectively. The values of these fitting parameters as obtained from the nonlinear least squares fit are $d_{15} = 624 \times 10^{-12}$ m/V, $f_{d_1} = 20.2$ kHz, and damping ratio $\zeta = 0.96$. The damping ratio calculated from modal analysis is 0.992 and the assumed value of d_{15} is 584×10^{-12} m/V. The first damped natural frequency obtained from experiments is 20.1 kHz and the shear displacement of the sensing element Δy in the above frequency response experiment at $\omega/\omega_{n_1} = 1$ is approximately 180 pm.

Drosophila melanogaster which is commonly known as the fruit fly or vinegar fly is used in the study of genetics, physiology, and life history evolution. Apart from the easy availability of these flies, the ease with which they can be bred and taken care of[29] is the reason why they are used in these studies. Mutated flies exhibit altered material properties compared to that of nonmutated flies. This implies a change in the density of the material and hence a change in the mass of the fly during the developmental stages. Although there is a difference in the mass during developmental stage, the mass of both types of fully grown fly is almost the same.[30,31]

The sensor developed is used to measure the mass of 20-day old and 40-day old drosophila flies as shown in Fig. 6. The same can also be used to measure the mass of drosophila egg and mass of larvae during its developmental stage. The fly placement on the sensor is done by means of a tweezer to measure its mass. The only concern in carrying out these experiments is that the drosophila would fly away when the experiments are conducted in open. Hence the flies were suitably etherized to restrict their movements during the period of measurement. The mean mass of the egg, larvae, and the drosophila are found to be 2.8 μg, 17.8 μg, and 213.6 μg, respectively. The 20-day drosophila fly has a mean mass of 205.1 μg, while the 40-day old drosophila fly measures 213.6 μg.

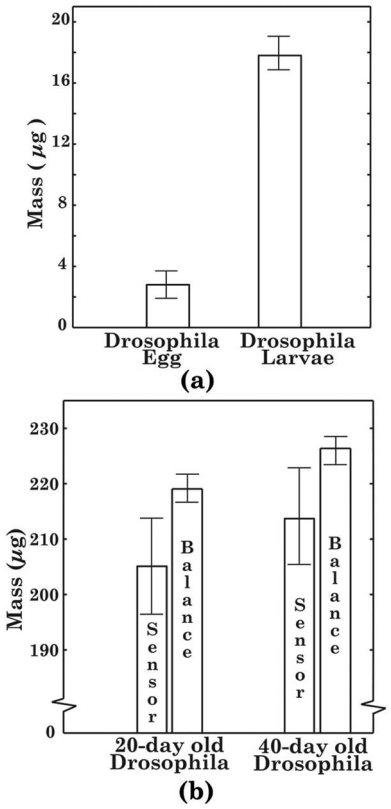

FIG. 6. Measured mass of drosophila fly. (a) Mass of drosophila egg and larvae. (b) Mass of 20-day old and 40-day old flies.

A sample size of 20 drosophila melanogaster flies was used to measure their mass in a vibrating tuning fork weighing balance. The mean mass of 20-day old and 40-day old drosophila flies as measured by the weighing balance were found to be 220 μg and 225 μg. As shown in Figs. 6(a) and 6(b) the difference in the mass of the drosophila fly, the egg, and larvae are 2 and 1 orders of magnitude. The non-resonant mass sensor can be used over this entire range just changing the input voltage V_{in} to suit the order of magnitude of the mass to be measured.

The standalone point of the frequency response of the sensor is the difference in the sensor voltage output voltage for solid mass and water. Now the question that needs to be addressed is, how much is the difference and how would it affect measurement of the mass of a viscoelastic/biological sample as in this case of drosophila fly, its egg and larvae. Fig. 7 shows the % error in the voltage output of the sensor. The results shown in Fig. 7 are from experiments conducted at an operating frequency of $f = 1000$ Hz. The input voltage to the sensor V_{in} is 5 V and the error in the measurement of the mass for a solid mass and water is found to be very close to 30% at $\omega/\omega_{n_1} = 1$,

$$\%\text{Error} = \left.\frac{V_{solid} - V_{visco}}{V_{solid}}\right|_{\omega/\omega_{n_1}} \times 100\%, \tag{12}$$

where V_{solid} is the voltage output of the sensor when solid mass is used and V_{visco} is the voltage output when a viscous/viscoelastic mass is used. V_{solid} and V_{visco} are measured by

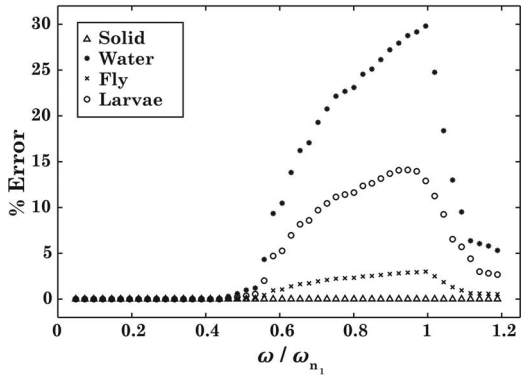

FIG. 7. Error in the mass measurement of solid, water, drosophila fly, and drosophila larvae over a frequency range of 1–25 kHz. The input voltage $V_{in} = 5\ V$ and the oscillation amplitude at $\omega/\omega_{n_1} = 1$ is 3 nm.

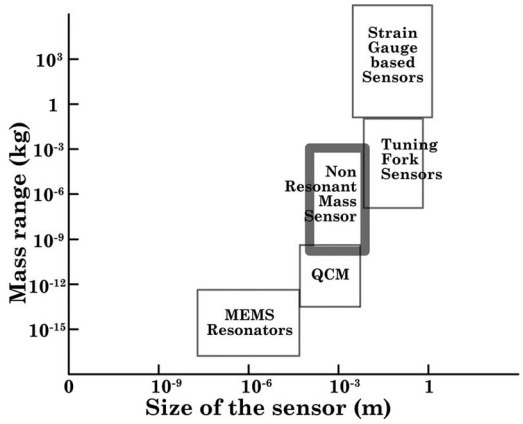

FIG. 8. A comparative study of various mass sensors with its measurement range.

experimental frequency sweep. The difference in the voltage output of the sensor is evident after the ratio of ω/ω_{n_1} becomes greater than 0.4.

The error approximation from (12) requires the frequency response of the sensor to be recorded for solid, water, drosophila fly, and larvae. The voltage output of the sensor for a given value of ω/ω_{n_1} is used in (12) to calculate the percentage of error in the measurement of the solid mass, water, drosophila fly, and its larvae. The masses of solid and water are 1 mg, while the drosophila fly and larvae measure 17.8 μg and 213.6 μg. The volume of the mass to be measured does not affect the measurement in the non-resonant mode. When the sensor is used at resonance, the difference in voltage output of the sensor is maximum for water. The response of the sensor when a drosophila fly is measured is similar to that of a solid and % error trend is close to the solid behavior. The response of the sensor when larvae is measured differs from the solid mass trend and lies in between that of solid mass and water. Thus the viscoelastic material property of the mass being measured affects the response and behavior of the sensor. This difference in the sensor output when used as a resonator gives a measurement that is not accurate. The underlying idea behind the work to overcome the difficulty of accounting for the viscosity induced "missing mass effect" of the mass to be measured can be realized here.

The voltage output of the sensor is dependent on the sensitivity of the charge amplifier. The maximum voltage output of the sensor after charge conversion is 12 V. Due to this measurement restriction in the overall experimental setup, the maximum value of the mass that can be measured is about 1 g. As given in (8), the voltage output of the sensor is a function of the operating frequency (f) as well. Hence, the sensitivity can be varied by varying operating frequency. Fig. 8 shows a comparative study of the existing mass measurement techniques with its range and resolution as well as its size. In principle, the strain gauge based mass measurement techniques are used in static mass measurement, while the resonant sensors are used in dynamic applications. Although, there is a difference in the working principle of sensing, a comparison of the range of mass measurement and its resolution against the size of the sensor indicates the use of non-resonant mass sensor in both static and dynamic mass measurements.

VI. CONCLUSIONS

A piezoelectric based non-resonant mass sensor for mass measurement of viscoelastic or biological specimens has been developed. The sensor is made of an actuator element that drives the sensor system, the sensing element does the mass measurement and gives an output based on the charge generated in the sensing element due to the induced shear strain. The damped natural frequencies obtained from the experiments are $f_{d_1} = 20.1$ kHz and $f_{d_2} = 49.4$ kHz. The calibration of the sensor was carried out with known solid and liquid mass (water with $\rho = 1000$ kg/m^3). The voltage output of the sensor increased with increasing lateral area and decreasing thickness of the piezos. The linearly swept frequency response curve showed a deviation in the voltage output of the sensor between solid and liquid mass for operating frequency $f > 8$ kHz. As seen in Fig. 5, the response of the sensor up to a ratio of $\omega/\omega_{n_1} = 0.4$ is independent of the damping. The sensor has a resolution of 0.1 μg and can be used to measure masses ranging from 0.1 μg to 1 g. Even though, the sensor is operated in a stiffness controlled region, it can also be used as a resonator.

Drosophila melanogaster (fruit fly) was used as the biological specimen whose mass was measured. 20-day old and 40-day old drosophila flies were used for measurement and a mean mass of 205.1 $\pm$ 8.2 μg and 213.6 $\pm$ 12.7 μg were found, respectively. The mass of the drosophila egg and the larvae during its developmental stage was found out to be 2.8 $\pm$ 0.9 μg and 17.8 $\pm$ 1.5 μg, respectively. The advantage of this sensor is the ease with which the sensitivity can be varied by varying the input voltage ranging from 1–300 V. The frequency response of the sensor showed a difference in the voltage output of the sensor when the ratio of $\omega/\omega_{n_1} \geq 0.4$ for water, drosophila fly, and larvae compared to solid. The behavior of the drosophila fly is more like a solid and the behavior of the larvae is more like a liquid and their behavior is in between that of a solid and a liquid. The damping effects due to viscosity/viscoelastic properties of the mass to be

measured and the surrounding medium of air can be reduced by a large extent the non-resonant mode of operation of the sensor as shown in the error calculations. The idea of utilizing stiffness controlled range for mass measurement has been clearly proved. Mass measurements eliminating the "missing mass" effect of biological samples can be carried out with this non-resonant piezoelectric based mass sensor.

ACKNOWLEDGMENTS

The authors would like to thank Professor K. R. Y. Simha for the fruitful discussions. The authors are immensely grateful to Dr. Upendra Nongthomba from Department of Molecular Reproduction, Development and Genetics for his insights and Anantheshwara K, Roshan T. John, and Lavanya Devi. A.L. from Force Microscopy Lab, Department of Mechanical Engineering, Indian Institute of Science. The authors are also thankful to Robert Bosch Centre for Cyber Physical Systems for partly funding this work.

[1]M. Tabib-Azar and A. Garcia-Valenzuela, "Sensing means and sensor shells: A new method of comparative study of piezoelectric, piezoresistive, electrostatic, magnetic, and optical sensors," Sens. Actuat. A **48**(2), 87–100 (1995).
[2]H. Golnabi, "Simple capacitive sensors for mass measurements," Rev. Sci. Instrum. **68**(3), 1613–1617 (1997).
[3]Z. Hu, J. Hedley, N. Keegan, J. Spoors, W. Waugh, B. Gallacher, F.-X. Boillot, J. Collet, and C. McNeil, "Design, fabrication and characterization of a piezoelectric mems diaphragm resonator mass sensor," J. Micromech. Microeng. **23**(12), 125019 (2013).
[4]A. G. Gibbs, A. K. Chippindale, and M. R. Rose, "Physiological mechanisms of evolved desiccation resistance in drosophila melanogaster," in *Methuselah Flies: A Case Study in the Evolution of Aging*, edited by M. R. Rose, H. B. Passananti, and M. Matos, (World Scientific, 2004), pp. 10–16.
[5]C. Fredriksson, S. Kihlman, M. Rodahl, and B. Kasemo, "The piezoelectric quartz crystal mass and dissipation sensor: A means of studying cell adhesion," Langmuir **14**(2), 248–251 (1998).
[6]A. P. Davila, J. Jang, A. K. Gupta, T. Walter, A. Aronson, and R. Bashir, "Microresonator mass sensors for detection of *Bacillus anthracis* Sterne spores in air and water," Biosens. Bioelect. **22**(12), 3028–3035 (2007).
[7]T. Thundat, E. A. Wachter, S. L. Sharp, and R. J. Warmack, "Detection of mercury vapor using resonating microcantilevers," Appl. Phys. Lett. **66**(13), 1695–1697 (1995).
[8]S. Chopra, A. Pham, J. Gaillard, A. Parker, and A. M. Rao, "Carbon-nanotube-based resonant-circuit sensor for ammonia," Appl. Phys. Lett. **80**(24), 4632–4634 (2002).
[9]P. Hauptmann, "Resonant sensors and applications," Sens. Actuat. A **26**(1), 371–377 (1991).
[10]J. Teva, G. Abadal, F. Torres, J. Verd, F. Pérez-Murano, and N. Barniol, "A femtogram resolution mass sensor platform, based on SOI electrostatically driven resonant cantilever. Part I: Electromechanical model and parameter extraction," Ultramicroscopy **106**(8), 800–807 (2006).
[11]J. Teva, G. Abadal, F. Torres, J. Verd, F. Pérez-Murano, and N. Barniol, "A femtogram resolution mass sensor platform based on SOI electrostatically driven resonant cantilever. Part II: Sensor calibration and glycerine evaporation rate measurement," Ultramicroscopy **106**(8), 808–814 (2006).
[12]Z. Shen, W. Y. Shih, and W.-H. Shih, "Mass detection sensitivity of piezoelectric cantilevers with a nonpiezoelectric extension," Rev. Sci. Instrum. **77**(6), 065101 (2006).
[13]B. E. DeMartini, J. F. Rhoads, S. W. Shaw, and K. L. Turner, "A single input–single output mass sensor based on a coupled array of microresonators," Sens. Actuat. A **137**(1), 147–156 (2007).
[14]I. Mehdipour and A. Barari, "Why the center-point of bridged carbon nanotube length is the most mass sensitive location for mass attachment?," Comput. Mater. Sci. **55**, 136–141 (2012).
[15]M. V. Voinova, M. Jonson, and B. Kasemo, "'Missing mass' effect in biosensor's QCM applications," Biosens. Bioelect. **17**(10), 835–841 (2002).
[16]R. B. Bhiladvala and Z. J. Wang, "Effect of fluids on the Q factor and resonance frequency of oscillating micrometer and nanometer scale beams," Phys. Rev. E **69**(3), 036307 (2004).
[17]M. Rodahl and B. Kasemo, "On the measurement of thin liquid overlayers with the quartz-crystal microbalance," Sens. Actuat. A **54**(1), 448–456 (1996).
[18]M. K. Jain and C. A. Grimes, "Effect of surface roughness on liquid property measurements using mechanically oscillating sensors," Sens. Actuat. A **100**(1), 63–69 (2002).
[19]W. Zhang and K. L. Turner, "Pressure-dependent damping characteristics of microsilicon beam resonators for different resonant modes," in *Proceedings of the IEEE Conference on Sensors* (IEEE, 2005), p. 4.
[20]H. Anderson, M. Jönsson, L. Vestling, U. Lindberg, and T. Aastrup, "Quartz crystal microbalance sensor design: I. Experimental study of sensor response and performance," Sens. Actuat. B **123**(1), 27–34 (2007).
[21]C. R. Kirkendall and J. W. Kwon, "Liquid damping isolation on quartz crystal microbalance for effective preservation of high quality factor and sensitivity in liquid," in *Proceedings of the IEEE Conference on Sensors* (IEEE, 2009), pp. 607–610.
[22]J. R. Davis, *Copper and Copper Alloys* (ASM International, 2001).
[23]S. D. Senturia, *Microsystem Design* (Springer, 2010).
[24]S. W. Or, H. L. W. Chan, and P. C. K. Liu, "Piezocomposite ultrasonic transducer for high-frequency wire-bonding of microelectronics devices," Sens. Actuat. A **133**(1), 195–199 (2007).
[25]E. Volterra and E. Charalampos Zachmanoglou, *Dynamics of Vibrations* (Merrill Books, Ohio, 1965).
[26]W. Thomson, *Theory of Vibration with Applications* (Prentice Hall, 1997).
[27]K. Kapoor, V. Kanawade, V. Shukla, and S. Patil, "A new tuning fork-based instrument for oscillatory shear rheology of nano-confined liquids," Rev. Sci. Instrum. **84**(2), 025101 (2013).
[28]M. Rodahl and B. Kasemo, "Frequency and dissipation-factor responses to localized liquid deposits on a QCM electrode," Sens. Actuat. B **37**(1), 111–116 (1996).
[29]J. H. Sang, "Drosophila melanogaster: The fruit fly," *Encyclopedia of Genetics* (Fitzroy Dearborn Publishers, 2001).
[30]M. B. Seiger, "The effects of chromosome substitution on male body weight of drosophila melanogaster," Genetics **53**(2), 237 (1966).
[31]R. R. Frahm and K.-I. Kojima, "Comparison of selection responses on body weight under divergent larval density conditions in drosophila pseudoobscura," Genetics **54**(2), 625 (1966).